



Ultimate fate of a dynamical bubble/droplet system following acoustic vaporization

Thomas Lacour, Tony Valier-Brasier, François Coulouvrat

► To cite this version:

Thomas Lacour, Tony Valier-Brasier, François Coulouvrat. Ultimate fate of a dynamical bubble/droplet system following acoustic vaporization. *Physics of Fluids*, 2020, 32 (5), pp.051702. 10.1063/5.0004375 . hal-02871138

HAL Id: hal-02871138

<https://hal.sorbonne-universite.fr/hal-02871138>

Submitted on 17 Jun 2020

HAL is a multi-disciplinary open access archive for the deposit and dissemination of scientific research documents, whether they are published or not. The documents may come from teaching and research institutions in France or abroad, or from public or private research centers.

L'archive ouverte pluridisciplinaire **HAL**, est destinée au dépôt et à la diffusion de documents scientifiques de niveau recherche, publiés ou non, émanant des établissements d'enseignement et de recherche français ou étrangers, des laboratoires publics ou privés.


Ultimate fate of a dynamical bubble/droplet system following acoustic vaporization

Cite as: Phys. Fluids **32**, 051702 (2020); <https://doi.org/10.1063/5.0004375>

Submitted: 01 March 2020 . Accepted: 29 April 2020 . Published Online: 15 May 2020

Thomas Lacour , Tony Valier-Brasier, and François Coulouvrat 

COLLECTIONS

 This paper was selected as Featured



View Online



Export Citation



CrossMark

ARTICLES YOU MAY BE INTERESTED IN

[Influence of glow discharge on evolution of disturbance in a hypersonic boundary layer: The effect of first mode](#)

Physics of Fluids **32**, 051701 (2020); <https://doi.org/10.1063/5.0008457>

[On coughing and airborne droplet transmission to humans](#)

Physics of Fluids **32**, 053310 (2020); <https://doi.org/10.1063/5.0011960>

[Dispersion of solute in straining flows and boundary layers](#)

Physics of Fluids **32**, 051703 (2020); <https://doi.org/10.1063/5.0010892>



NEW: TOPIC ALERTS

Explore the latest discoveries in your field of research

SIGN UP TODAY!


Ultimate fate of a dynamical bubble/droplet system following acoustic vaporization

Cite as: Phys. Fluids 32, 051702 (2020); doi: 10.1063/5.0004375

Submitted: 1 March 2020 • Accepted: 29 April 2020 •

Published Online: 15 May 2020



Thomas Lacour,^{a)}  Tony Valier-Brasier,^{b)} and François Coulouvrat^{c)} 

AFFILIATIONS

Sorbonne Université, CNRS, UMR 7190, Institut Jean Le Rond d'Alembert, Paris, France

^{a)} Author to whom correspondence should be addressed: tmlacour@gmail.com

^{b)} Electronic mail: tony.valier-brasier@sorbonne-universite.fr

^{c)} Electronic mail: francois.coulouvrat@sorbonne-universite.fr

ABSTRACT

The phase-change of a liquid droplet induced by a supply of acoustic energy is known as “Acoustic Droplet Vaporization,” and it represents a versatile tool for medical applications. In an attempt to understand the complex mechanisms that drive the vaporization threshold, a theoretical concentric three phase model (bubble of vapor dodecafluoropentane + layer of liquid dodecafluoropentane + water) is used to compute numerical simulations of the vapor bubble time evolution. The dynamics are sorted into different regimes depending on their shared characteristic and the system ultimate fate. Those regimes are then organized within a phase diagram that collects all the possible dynamics and that predicts whether the complete vaporization occurs or not.

Published under license by AIP Publishing. <https://doi.org/10.1063/5.0004375>

Some innovative medical tools for diagnosis and therapy of malignant diseases used the vaporization of metastable emulsions of biocompatible liquid nanodroplets using ultrasound:^{1,2} the acoustic droplet vaporization (ADV). This phenomenon is carried out by an adequate supply of acoustic energy to a liquid droplet. Optical observations of the ADV outline a highly nonlinear dynamics with a strong sensitivity to the experimental configuration and noteworthy to the acoustic frequency and pressure.^{3–5} Numerous experimental studies endeavored to determine the acoustic pressure threshold necessary to reach complete vaporization. However, no clear trend regarding frequency is yet available to predict the optimum parameters (see Table in Ref. 6). Some authors observed a threshold decreasing with frequency,^{7–9} whereas others found the opposite behavior.^{5,6,10} These discrepancies are the evidence of the richness and complexity of the vaporization mechanism. The prediction of the ADV threshold is therefore essential to optimize its efficiency.

The ADV is usually modeled as a concentric three phase system (see Fig. 1), made of a centered vapor bubble already nucleated, surrounded by a layer of the same species in its liquid state, and immersed in pure water (no dissolved species or gases) at body temperature. Note that this system cannot be at equilibrium even when no acoustic field is supplied. When the nucleus radius is above a critical value, the vapor phase naturally grows by evaporation;

otherwise, it shrinks and disappears due to condensation (see Fig. 2 in Ref. 11). The ADV process amounts to counterbalance this natural collapse by applying an acoustic expansion. The liquid/vapor mixture is composed of dodecafluoropentane (C_5F_{12} or DDFP), a promising candidate for its low bulk boiling point¹² (29 °C). It nevertheless remains in a metastable liquid phase because of the additional Laplace pressure at the interface. The static pressure p_0 is modulated by a continuous harmonic excitation beginning by an expansion $p(t) = p_0 - p_a \sin(2\pi ft)$, for $t > 0$, where p_a is the acoustic amplitude. A more realistic excitation would involve nonlinear distortion, harmonic generation, shock formation, and asymmetrical waveform.¹³ This would imply to consider many more parameters, would make the ADV landscape even more intricate, and would deserve further studies. However, note that the corresponding superfocusing effect⁴ has been observed only for droplets larger than 6 μm .

In our previous numerical studies,^{11,14} the ADV output has been classified into three regimes of evolution: irreversible collapse of the vapor bubble, complete vaporization of the droplet, and intermediate behaviors. These studies were performed for nanometric and micrometric DDFP droplets encapsulated within a viscoelastic shell with linear¹¹ and nonlinear¹⁴ elasticity excited up to 10 MHz and 10 MPa. The initial radius of the vapor nucleus ranged

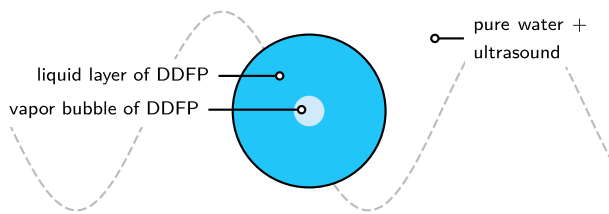


FIG. 1. Sketch of the system geometry.

between 40 nm and 80 nm. A phase diagram has been proposed that maps these regimes in the frequency/amplitude plane, where boundaries between regimes define at least two thresholds (bubble growth and direct vaporization). A similar representation is proposed by Cho and Son¹⁵ by means of a level set interface tracking method. The objective of this letter is to further investigate the intermediate regime and therefore clarify the experimental studies about the ADV threshold. The concept of vaporization threshold appears more complex than usually thought at least in the high frequency regime. The highly nonlinear time evolution of a vapor bubble within a droplet, with possible multiple rebounds and high temperatures, explains the richness of this intermediate regime.

We here rely on the model of Doinikov *et al.* that was successfully validated for two chemical species of much lower bulk point in comparison with optical measurements for micrometric droplets.^{16,17} The generalized Rayleigh–Plesset equation is numerically solved with an adaptive step solver suitable for stiff equations. The coupled heat transfer problem is solved outside the bubble in a transformed coordinate system using second order finite differences,¹¹ which is shown to be equivalent to a spectral collocation method.¹⁸ The temperature of the vapor phase is assumed to be uniform, as justified by large diffusion lengths in the gas compared to the liquids. At the initial time, the droplet radius is 1 μm , the smallest size for which observations of the ADV process for individual particles are available.¹⁶ Even if the vapor behavior strongly depends on the nucleus size at the initial time (for sensitivity to this parameter, see Ref. 14), its value is here arbitrarily fixed to $R(t=0) = 80$ nm (below the critical value separating the spontaneous collapse from the spontaneous vaporization). This value is one order of magnitude larger compared to the classical nucleation theory (CNT) but is acceptable as a coalesced cluster of bubbles or a single growing nucleus. Note that CNT has been applied to model ADV¹³ with encouraging results regarding the ADV threshold at least for large droplets, but CNT, nevertheless, remains in some cases contradictory with the frequency dependence of this threshold (as discussed in Ref. 19). We thus restrict our study to the influence of acoustical parameters: frequency f and amplitude p_a . Acoustic modulation starts with a rarefaction phase to favor a volumic expansion of the vapor nucleus. The computation is stopped either when the bubble radius lowers beneath $R_0/100 = 0.8$ nm (irreversible collapse) or when the thickness of the liquid layer of dodecafluoropentane reaches 0 *modulo* the computer precision (complete vaporization). These criteria have been modified, and it turns out to they have little (almost no) sensitivity on the ultimate fate of the system. To consolidate our results and test the robustness of the model, the numerical convergence has first to be checked.

Time evolutions of the bubble radius are illustrated by Fig. 2 for seven values of the amplitude p_a at 6 MHz frequency. A wide range of dynamics is obtained. At least three regimes can be systematically identified: a fast and irreversible collapse of the bubble without any growth (regime I, Fig. 2 at 312.5 kPa), a direct and complete vaporization without any rebounds (regime III, Fig. 2 at 7 MPa), and intermediate behaviors (regime II) with other features (multiple rebounds, oscillations, or partial vaporization) now detailed. Note that in Fig. 2, the bubble radius is out of phase with acoustic forcing at the beginning of the process, but both rapidly tune with one another in about one cycle.

Regime II begins necessarily with a growth of the vapor bubble, followed by a recondensation that might lead to various *scenarios*, depending on the initial conditions. Between regimes I and III, two collapsing regimes are well discriminated from other ones: regime IIa with one maximum (see Fig. 2 at 1 MPa) and regime IIb with two maxima (see Fig. 2 at 4 MPa). Between regimes IIa and IIb, multiple rebounds can arise before a complete vaporization or an irreversible collapse, depending on a subtle competition mainly between the surface tension, the heat transfer, and the acoustic modulation. A vaporization situation is obtained through regime IIc: the bubble grows up to a local maximum, then recondenses and rebounds one time before

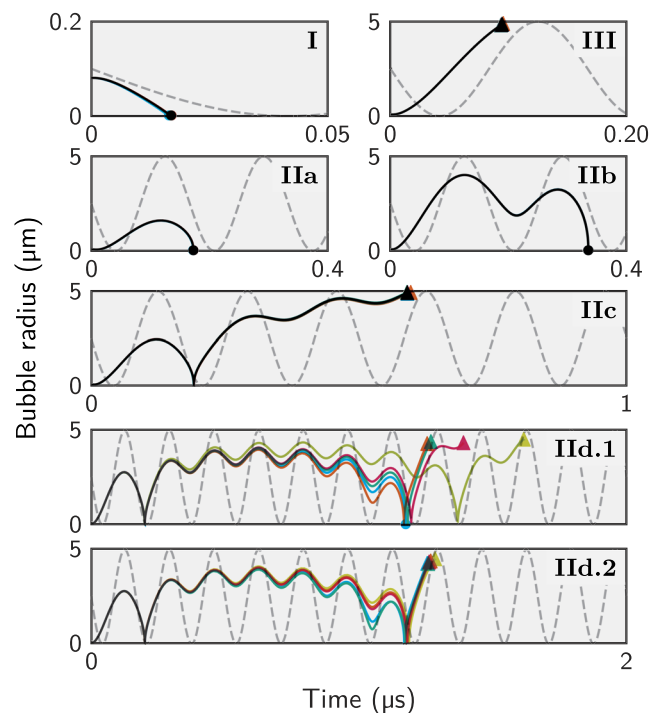


FIG. 2. Convergence and regimes for the bubble dynamics. Bubble radius vs time for one harmonic acoustic excitation (dashed lines, amplitude in arbitrary units) at 6 MHz and peak negative pressure: 312.5 kPa (I), 7 MPa (III), 1 MPa (IIa), 4 MPa (IIb), 1.8 MPa (IIc), 2.18 MPa (IIId.1), and 2.19 MPa (IIId.2). Each box superimposes several curves of the dynamics for different numbers of discretization points per thermal diffusion length (8 in yellow, 16 in blue, 32 in green, 64 in orange, and 128 in red). Black means superimposed colors and thus indicates convergence. A bullet (●) denotes an irreversible collapse, whereas a triangle (▲) is a complete vaporization.

smoothly oscillating, and finally completely vaporizes (Fig. 2 at 1.8 MPa). Between regimes IIc and IIb, even more complex situations are observed. For example, complete vaporization is obtained after oscillations occurring between two violent rebound events (Fig. 2, regime IId).

For each case, convergence is shown by increasing the number of points ($N = 2^n$ with $n = 3, 4, \dots, 8$) per unit of thermal diffusion length used to discretize the heat equation [see Eq. (20) in Ref. 16]. For regimes I, IIa, IIb, IIc, and III, the numerical convergence is ensured because no noticeable difference in the dynamics is visible. The model and its spatial temperature discretization, therefore, succeed to give a reproducible solution over the selected range of N . Only for regime IId, the bubble fate, although invariant, can be inaccurate in time. When the temperature is insufficiently sampled (see IId.1 for $N = 8$), the second rebound can be delayed compared to finer resolutions. If the value of N is too low, collapse can be predicted instead of complete vaporization (see IId.1 for $N = 16$). This extreme sensitivity stands out only for regime IId (compare IId.1 and IId.2 in Fig. 2), which is linked to multiple rebounds. Indeed, the uniform temperature assumption within the vapor phase is likely to explain the rebound inaccuracy: the mass flux is assumed to be proportional to the heat flux.^{16,18} Taking into account the whole diffusion problem within the vapor phase¹⁸ would improve the model in future work. However, the value $N = 32$ enables us to reach numerical convergence for the ultimate fate of the bubble (collapse or vaporization). This value is chosen in the following.

To better understand regime II and its boundaries with regimes I and III, the maximum bubble surface is displayed in Fig. 3 as a function of the amplitude of the acoustical excitation for 1 MHz and 6 MHz. The ultimate fate of the bubble (vaporization or collapse) is also pointed out. Note that in case of vaporization, the bubble goes on growing up, as shown by Doinikov *et al.*¹⁶ The maximum bubble surface depends on both the amplitude and the frequency. A low frequency behavior is observed for 1 MHz with a sharp discontinuity of the maximum surface with the amplitude. Below

3.2 MPa, the bubble collapses (regime I). Above 3.2 MPa, vaporization is obtained (regime III) with a maximum bubble radius approaching $5 \mu\text{m}$ ($314 \mu\text{m}^2$ for the surface), which is the usual factor for the phase change of one micrometer DDFP droplet using the perfect gas law: $(\rho_\ell/\rho_v)^{1/3} \approx 5.05$. For such a low frequency, the vaporization threshold is clearly defined. For higher frequencies [Fig. 3 (b)], the transition between regimes I and III is now made through regime II. Regime I still exists but on a shorter range. The time rate of pressure change is higher and succeeds to counterbalance the natural trend of the nucleus to collapse due to surface tension. Then, the bubble growth is possible, and complete vaporization is achieved because the acoustic rarefaction phase is sufficiently long. Between regimes I and III, the maximum bubble surface tends to be linearly dependent on the amplitude of excitation, except within a short range where sharp variations are observed. This linearity (II.a and II.b) is probably due to surface processes such as phase change at the interface, heat diffusion, or surface tension effect. In the short interval between 1.7 MPa and 2.3 MPa, vaporization can happen, but its distribution is not continuous. Such a representation displayed in Fig. 3 gives a clear repartition of the different bubble dynamics and implicitly involves the notion of the threshold between the different regimes. The lowest pressure value necessary for regime III (monotonic dynamics without any rebounds) is what we previously called the direct threshold.¹⁴ The lowest pressure value for regime II (at least a growth to one maximum) or the highest for regime I is the growth threshold.¹¹ This serves as an introduction to the phase diagram that deals with such a repartition in the full frequency/pressure plane.

Other quantities can be calculated as useful indicators to discriminate the different regimes and especially subregimes within regime II. The vaporization dynamics is therefore computed for a regular grid (160×160) of values in the frequency/pressure plane. Using all these simulations, physical parameters are computed: the final bubble radius [in μm , Fig. 4(a)], the final time of the dynamics [in μs , Fig. 4(b)], the maximum bubble surface temperature [in MK, Fig. 4(c)], and the number of rebounds [Fig. 4(d)]. These diagrams showing closed areas allow us to accurately discriminate the different regimes.

The final bubble radius extracted from all simulations lies in the range $0\text{--}6 \mu\text{m}$ [Fig. 4(a)]. Smallest values near $0 \mu\text{m}$ correspond to a final collapse situation. Highest values are associated with a complete vaporization. Intermediate values do exist (thin bottom line at 5 kPa), but they are not relevant because they are incomplete dynamics for which the computation has been stopped too early.

The final bubble radius makes distinguishing regime III in the upper closed area possible (see the small scheme on the corner). To exhibit subregimes within the white area (collapse), we need other indicators. The values of the final time of the dynamics enable us to discriminate two other regimes [Fig. 4(b)]: regimes IIa and I. The boundaries are sufficiently sharp to clearly identify these fast regimes from the slowest ones. Looking at the temperature [Fig. 4(c)], we outline cold dynamics (white area) and hot ones. High values of the maximum bubble radius are linked to a violent collapse (see Fig. 3). For regime IIb (two maxima and a final collapse), the temperature is hotter than for other regimes, thus allowing us to separate this one [see the small graphic in Fig. 4(c)]. Finally, the number of rebounds [Fig. 4(d)], which is above zero only for a small fraction of regime II, discriminates the last converged regime: regime IIc (only

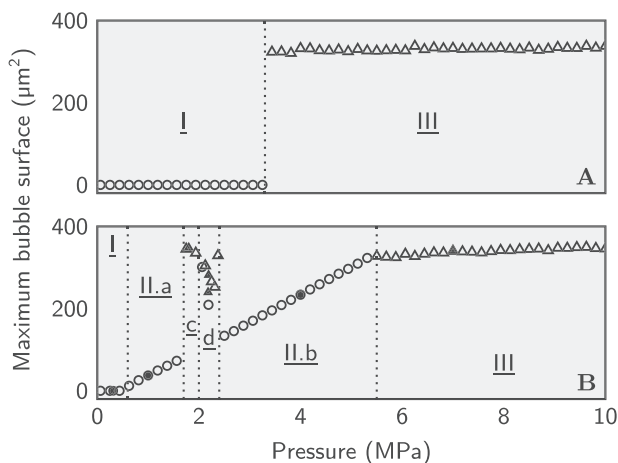


FIG. 3. Maximum bubble surface versus peak negative pressure during vaporization dynamics for two frequencies: (a) 1 MHz and (b) 6 MHz. Triangles denote vaporization events, and bullets denote irreversible collapses of the vapor bubble. Full black symbols in B are cases of Fig. 2.

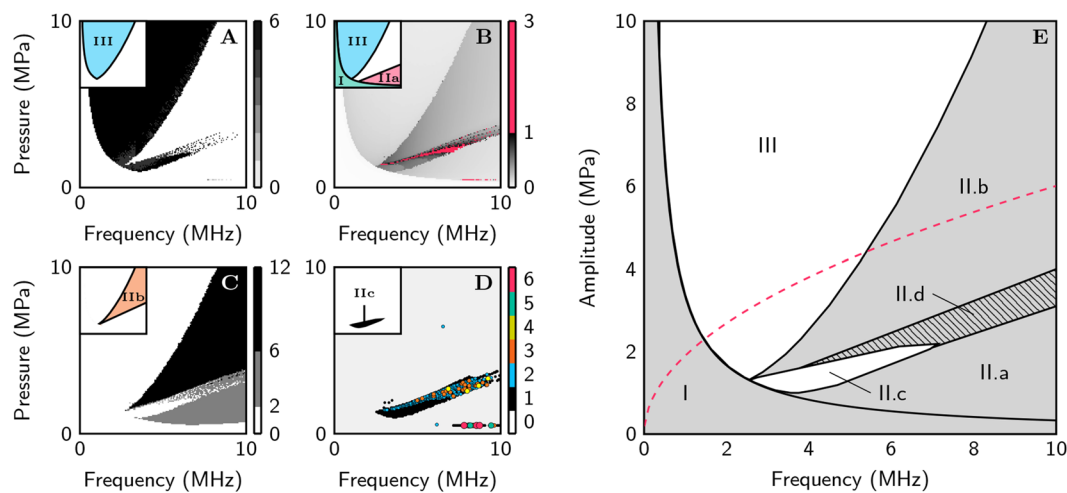


FIG. 4. Phase diagram of a single bubble/droplet system fate during acoustic droplet vaporization. (a) Final bubble radius (μm). (b) Final time of the numerical solution (μs). (c) Maximum bubble surface temperature (MK). (d) Number of rebounds. (e) Full phase diagram. Each small graph at the left top corner is the deduced regime. The dashed line on (e) is the mechanical index approved by FDA for diagnostic ultrasounds.

one rebound and complete vaporization). The remaining regime II_d (two or more rebounds with collapse or vaporization) lies between regimes II_a, II_b, and II_c but is not regularly distributed. Moreover, it is not fully reliable because of issues in numerical convergence, probably due to an incomplete heat description inside the vapor phase during the collapse, as previously discussed.

Different evolutions for the bubble dynamics are computed and systematically classified into discriminated regimes depending on their ultimate fate. Three regimes are observed: irreversible collapse (regime I), direct vaporization (regime III), and intermediate behaviors (regime II) that are the purpose of this letter. Using the final bubble radius, the final time of the dynamics, the maximum surface temperature, and the number of rebounds, we are able to construct a full phase diagram collecting all regimes in the frequency/amplitude domain [Fig. 4(e)]. The definitions and relevant characteristics of regimes are summarized in Table I. Vaporization events are associated with the growth of the vapor bubble and the “cold” dynamics. The collapse regimes II_a and II_b are the hottest ones because of the strong contraction of the vapor, following a maximum expansion (one maximum for II_a and two for II_b).

TABLE I. Characteristics of the different regimes.

Regime	End	Period	Temperature	Maxima	Rebound
I	Col.	<1/2	Cold	=0	=0
II _a	Col.	≈1	Hot	=1	=0
II _b	Col.	≈2	Hot	=2	=0
II _c	Vap.	>2	Cold	≥1	=1
II _d	?	>2	?	≥1	>1
III	Vap.	<1	Cold	=1	=0

To ensure the complete vaporization of the droplet, the acoustic parameters have to be chosen in either regime II_c or III. Note that both of them are partly (III) or totally (II_c) below the U.S. Food and Drug Administration (FDA) mechanical index limit allowed for diagnostic. Regime II_c allows reaching vaporization at the moderate amplitude using the benefit of a not too violent rebound and turns out of interest for applications. For selected parameters, it extends over a 4.5 MHz frequency range but is quite narrow in the pressure amplitude. Its possible widening could be further studied by smoothing the rebounds, including both models and experiments, the influence of encapsulation, dissolved gases, or surfactants. Moreover, rebounds need more accurate description by fully modeling heat transfers within the vapor phase. In addition, the common assumption of a centered vapor seed obviously simplifies the theoretical model. It is however observed, at least for large micrometric particles, that the nucleus is not always centered.^{4,20} Nevertheless, much of the dynamics of the ADV is governed by the bubble dynamics, only the volume of liquid to be vaporized playing a role, as discussed in Ref. 14. Decentering would therefore affect mostly the ultimate stage of the complete vaporization process when the bubble surface approaches the droplet one. One can reasonably think that most of the overall scheme here described remains mostly unchanged by decentering although this conjecture would need a specific study.

This work was supported by Plan Cancer 2014–2019 (www.plan-cancer.gouv.fr) as part of a research project in Physics, Mathematics, and Engineering Sciences Applied to Cancer Research.

DATA AVAILABILITY

The data that support the findings of this study are available from the corresponding author upon reasonable request.

REFERENCES

- ¹K. Loskutova, D. Grishenkov, and M. Ghorbani, "Review on acoustic droplet vaporization in ultrasound diagnostics and therapeutics," *BioMed Res. Int.* **2019**, 9480193.
- ²H. Lea-Banks, M. A. O'Reilly, and K. Hynnen, "Ultrasound-responsive droplets for therapy: A review," *J. Controlled Release* **293**, 144–154 (2019).
- ³O. D. Kripfgans, M. L. Fabiilli, P. L. Carson, and J. B. Fowlkes, "On the acoustic vaporization of micrometer-sized droplets," *J. Acoust. Soc. Am.* **116**, 272–281 (2004).
- ⁴O. Shpak, M. Verweij, H. J. Vos, N. de Jong, D. Lohse, and M. Versluis, "Acoustic droplet vaporization is initiated by superharmonic focusing," *Proc. Natl. Acad. Sci. U. S. A.* **111**, 1697–1702 (2014).
- ⁵P. S. Sheeran, T. O. Matsunaga, and P. A. Dayton, "Phase-transition thresholds and vaporization phenomena for ultrasound phase-change nanoemulsions assessed via high-speed optical microscopy," *Phys. Med. Biol.* **58**, 4513–4534 (2013).
- ⁶M. Aliabouzar, K. N. Kumar, and K. Sarkar, "Acoustic vaporization threshold of lipid-coated perfluoropentane droplets," *J. Acoust. Soc. Am.* **143**, 2001–2012 (2018).
- ⁷K. C. Schad and K. Hynnen, "In vitro characterization of perfluorocarbon droplets for focused ultrasound therapy," *Phys. Med. Biol.* **55**, 4933 (2010).
- ⁸P. S. Sheeran, V. P. Wong, S. Luois, R. J. McFarland, W. D. Ross, S. Feingold, T. O. Matsunaga, and P. A. Dayton, "Decafluorobutane as a phase-change contrast agent for low-energy extravascular ultrasonic imaging," *Ultrasound Med. Biol.* **37**, 1518–1530 (2011).
- ⁹R. Williams, C. Wright, E. Cherin, N. Reznik, M. Lee, I. Gorelikov, F. S. Foster, N. Matsuura, and P. N. Burns, "Characterization of submicron phase-change perfluorocarbon droplets for extravascular ultrasound imaging of cancer," *Ultrasound Med. Biol.* **39**, 475–489 (2013).
- ¹⁰A. L. Martin, M. Seo, R. Williams, G. Belayneh, F. S. Foster, and N. Matsuura, "Intracellular growth of nanoscale perfluorocarbon droplets for enhanced ultrasound-induced phase-change conversion," *Ultrasound Med. Biol.* **38**, 1799–1810 (2012).
- ¹¹M. Guédra and F. Coulouvrat, "A model for acoustic vaporization of encapsulated droplets," *J. Acoust. Soc. Am.* **138**, 3656–3667 (2015).
- ¹²T. Xu, Z. Cui, D. Li, F. Cao, J. Xu, Y. Zong, S. Wang, A. Bouakaz, M. Wan, and S. Zhang, "Cavitation characteristics of flowing low and high boiling-point perfluorocarbon phase-shift nanodroplets during focused ultrasound exposures," *Ultrason. Sonochem.* **65**, 105060 (2020).
- ¹³C. J. Miles, C. R. Doering, and O. D. Kripfgans, "Nucleation pressure threshold in acoustic droplet vaporization," *J. Appl. Phys.* **120**, 034903 (2016).
- ¹⁴T. Lacour, M. Guédra, T. Valier-Brasier, and F. Coulouvrat, "A model for acoustic vaporization dynamics of a bubble/droplet system encapsulated within a hyperelastic shell," *J. Acoust. Soc. Am.* **143**, 23–37 (2018).
- ¹⁵S. Cho and G. Son, "Numerical study of droplet vaporization under acoustic pulsing conditions," *J. Mech. Sci. Technol.* **33**, 1673–1680 (2019).
- ¹⁶A. A. Doinikov, P. S. Sheeran, A. Bouakaz, and P. A. Dayton, "Vaporization dynamics of volatile perfluorocarbon droplets: A theoretical model and in vitro validation," *Med. Phys.* **41**, 102901 (2014).
- ¹⁷O. Shpak, T. J. Kokhuis, Y. Luan, D. Lohse, N. de Jong, B. Fowlkes, M. Fabiilli, and M. Versluis, "Ultrafast dynamics of the acoustic vaporization of phase-change microdroplets," *J. Acoust. Soc. Am.* **134**, 1610–1621 (2013).
- ¹⁸A. Prosperetti, "Vapor bubbles," *Annu. Rev. Fluid Mech.* **49**, 221–248 (2017).
- ¹⁹M. Aliabouzar, K. N. Kumar, and K. Sarkar, "Effects of droplet size and perfluorocarbon boiling point on the frequency dependence of acoustic vaporization threshold," *J. Acoust. Soc. Am.* **145**, 1105–1116 (2019).
- ²⁰D. S. Li, O. D. Kripfgans, M. L. Fabiilli, J. Brian Fowlkes, and J. L. Bull, "Initial nucleation site formation due to acoustic droplet vaporization," *Appl. Phys. Lett.* **104**, 063703 (2014).